CONSTITUTIVE MODELS FOR COHESIVE ZONES IN MIXED MODE FRACTURE OF QUASI-BRITTLE MATERIALS

Luciani N. Lens, lnlens@unioeste.br
Centro de Ciências Exatas e Tecnológicas, Universidade Estadual do Oeste do Paraná, Campus de Cascavel, Rua Universitária 2069, Cascavel, PR, 85819-110, Brazil

Eduardo Bittencourt, eduardo.bittencourt@ufrgs.br
Virgínia M. R. d'Avila, vichy@ufrgs.br
Departamento de Engenharia Civil, Universidade Federal do Rio Grande do Sul, Av. Osvaldo Aranha 99, Porto Alegre, RS, 90035-190, Brazil

Abstract. *Discrete mixed mode fracture (modes I and II) of quasi-brittle materials is investigated using a coupled and an uncoupled cohesive zone constitutive model. Considering that finite element meshes used are not adapted during analysis, cracks do not coincide exactly with principal planes of stress, resulting shear traction components in crack cohesive zones. In this context, to simulate correctly the fracture process, mixed mode models must reduce such components promoting inelastic sliding. Numerical simulations indicate that mode II parameters are irrelevant in this regard. Actually, if non-associated plasticity is assumed, even the shape of yielding/cracking surfaces is negligible. Comparisons with experiments validate these observations.*

Keywords*: Quasi-brittle material, Cohesive zone models, Finite element analysis, Mixed mode fracture*

1. INTRODUCTION

In discrete fracture models, crack tip and associated singularities are present. In a finite element context, crack orientation can remain restricted to inter-element boundaries (Xu and Needleman, 1994, Camacho and Ortiz, 1999, etc). These models may induce certain mesh bias, but are quite simple to implement and their use is widely disseminated. They will be followed in the present work to simulate quasi-brittle rupture, in the context of the cohesive zone methodology (Xu and Needleman, 1994).

Different mixed mode fracture (modes I and II) models for quasi-brittle materials can be found in the literature (see Tijssens et al. 2000, Basche 2007, as examples). However, mode II properties are considered in general to have small importance on the fracture process (Jenq and Shah, 1988, Bocca et al., 1990, etc). For this reason, works such as Bocca et al. (1990) and Cendon et al. (2000) use pure mode I models to simulate mixed rupture. In these cases, cracks faces are continuously following the principal planes of stress (perpendicularly to the greatest traction) through adaptive mesh methods. Others, such as Cervenka (1994) and Gálvez et al. (2002), include also a mode II model. When adaptive meshes are not used, however, mode II considerations must be introduced in order to deal with shear effects that inevitably will appear in the crack cohesive zones.

In this work the interrelation between mixed mode models and shear traction components of the cohesive zones is investigated. Two limit cases to handle shear are studied here. These surfaces will be denoted as cracking surfaces. Any other cracking surface should be an intermediate case of these two. Double-edge notched (DEN) plates are analyzed to validate the proposed models. As no remeshing is used in the analyses and meshes are relatively coarse, cracks are forced to grow in planes where shear is present. It is demonstrated that the mixed mode constitutive model must handle this shear in order to achieve good fitting with experiments.

References to normal and tangential (shear) directions throughout the present text always refer to a local reference system linked to the crack cohesive surface. Crack opening is defined as w and is decomposed in an elastic part (w_e) and an inelastic part (w_i). Sliding of crack surfaces is defined as ν and also decomposed in an elastic and inelastic part (ν_e and ν_i, respectively). The models are intended to represent only fracture in tension and were implemented in the finite element code METAFOR. Constitutive model for volumetric finite elements used in the present formulation is elastic-linear.

The paper is organized as follows: the two mixed mode models introduced are detailed in section 2. Numerical simulations are shown in section 3 and discussions and final remarks are stated in section 4.

2. MIXED MODE FRACTURE MODELS

In this section, a description of constitutive models for pure modes I and II is firstly reviewed and then two mixed mode fracture models are introduced. The first is coupled and corresponds to a lower-bound for the cracking surfaces, while the second is uncoupled and corresponds to an upper-bound.

2.1. Constitutive models for pure modes I and II

The maximum normal traction (σ_{max}) of the cohesive zone is a function of the inelastic crack opening (w_i) and presents a softening. The softening curves shown in Fig. 1 are well-known models taken from the literature.

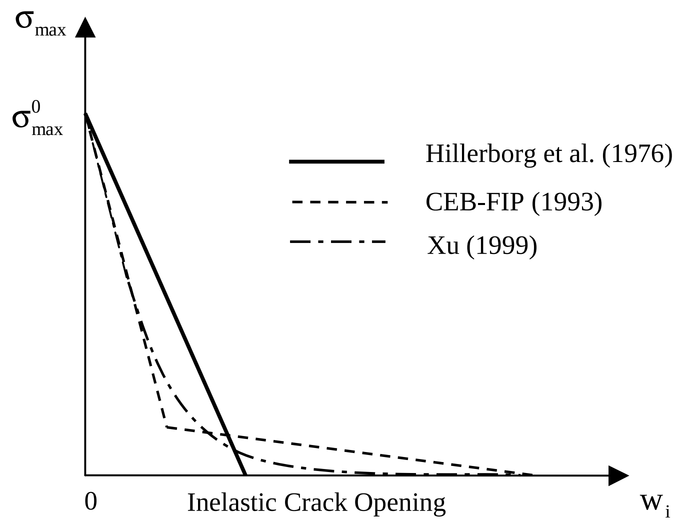

Figure 1. Normal traction softening for different relations.

The softening is linked to the development of the process zone where many complex phenomena, such as micro-cracking and interlock bridging, occur. The area under the curve is considered the specific fracture energy for mode I (G_{IC}) and the maximum normal traction for undamaged material (σ^0_{max}) is related to the material tensile strength. According to Carpinteri et al. (2003), it should range from 1 to 3 times the average tensile strength of the material, f_{tm}. The constitutive law for pure mode I can be considered as the Rankine theory. This model was used in mixed mode simulations where shear components were absent of the crack cohesive zone (Bocca et al. (1990) and Cendon et al. (2000)).

Quasi-brittle rupture in pure mode II has been also reported (Bažant and Pfeiffer, 2006), although not usual. Information regarding mode II properties is in general unavailable, except by indirect observation. It is believed that τ_{max} is greater or equal than σ_{max} (Gálvez et al., 2002) and specific fracture energy for mode II (G_{IIC}) is greater or equal than G_{IC} (Bažant and Pfeiffer, 2006, Carpinteri et al., 1993, etc). Due to the lack of information, the relation between τ and ν used is usually assumed to have the same shapes of its normal counterpart. The constitutive law for pure mode II can be seen as the Guest-Tresca theory.

2.1. The lower-bound (coupled) model

A coupled model is here defined by the Coulomb law with adherence, being adherence initially σ^0_{max}. The cracking surface assumes the shape depicted in Fig. 2. When damage occurs, cracking surface moves toward the left. Friction angle ϕ permits to determine τ_{max}, once σ_{max} is known. The cracking surface represented in Fig. 2 can be also considered a yield surface and analogies with plasticity can be built. According to Drucker's postulate of convexity, the Coulomb surface can be regarded as a lower-bound limit in tension. Cracking surface F in this case is defined as

$$F = |\tau| + (\sigma - \sigma_{max}) tan\,\phi = 0 , \tag{1}$$

with σ_{max} initially equal to σ^0_{max}. To update the value of σ_{max}, softening relations depicted in Fig. 1 are used, but are considered a function of an effective inelastic displacement (u_i^{eff}) rather than w_i. The value of u_i^{eff} is defined in Eq. (2) below:

$$u_i^{eff} = \sqrt{w_i^2 + \beta \nu_i^2} , \tag{2}$$

where β is a coupling factor between opening and sliding. This is a relatively simple coupled model when compared to others and only requires two coupling factors (ϕ and β).

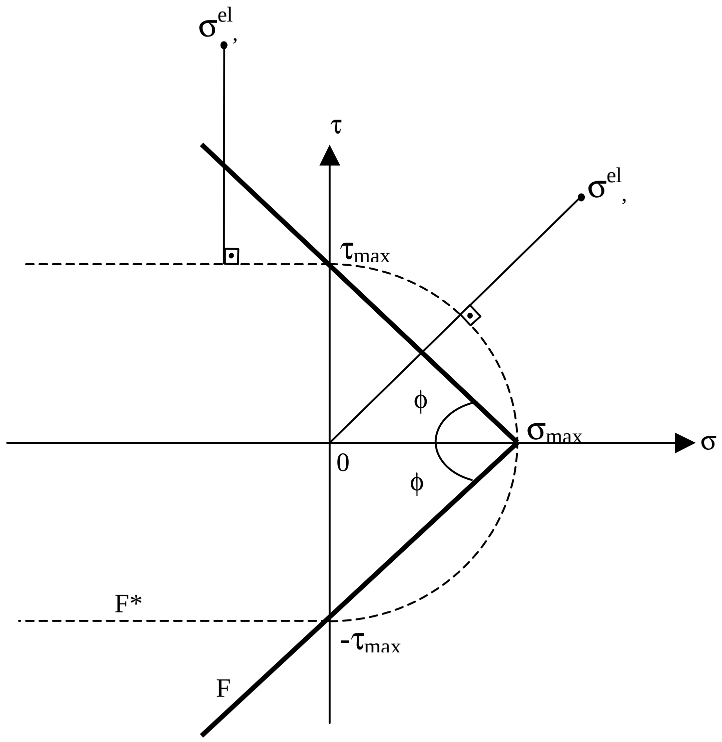

Figure 2. Lower-bound surface (*F*), plastic potential (*F**) and ineslastic displacement directions.

In cases where $F<0$ tractions are elastic and for $F=0$ damage or cracking is occurring. For F>0, stresses must return to the surface. An elastic-predictor, plastic-corrector type of algorithm is used. Elastic-predictor is given by Eq. (3),

$$\begin{Bmatrix} \sigma^{el} \\ \tau^{el} \end{Bmatrix} = \begin{bmatrix} K_n & 0 \\ 0 & K_t \end{bmatrix} \begin{Bmatrix} w \\ v \end{Bmatrix}, \tag{3}$$

where K_n and K_t are the normal and tangential elastic stiffness of the cohesive interface, respectively. Their values are defined as follows:

$$K_n = E\frac{\alpha}{l_c}, \qquad K_t = \mu\frac{\alpha}{l_c}. \tag{4}$$

l_c is the characteristic length scale of the finite element mesh and α is a constant (typically smaller than one).

Plastic-corrector can be written according to Eq. (5):

$$\begin{Bmatrix} \sigma \\ \tau \end{Bmatrix} = \begin{Bmatrix} \sigma^{el} \\ \tau^{el} \end{Bmatrix} - \begin{Bmatrix} K_n \\ K_t \end{Bmatrix} \int_{\Delta t} \begin{Bmatrix} \dot{w}_i \\ \dot{v}_i \end{Bmatrix} dt, \tag{5}$$

where t is time and Δt is the time-step used for integration. A non-associated plasticity will be assumed here, which means that inelastic displacements are not normal to cracking surface *F*. Instead, they are normal to a plastic potential *F**. The inelastic displacements are calculated as follows:

$$\begin{Bmatrix} \dot{w}_i \\ \dot{v}_i \end{Bmatrix} = \dot{\lambda} \begin{Bmatrix} \partial F^* / \partial \sigma \\ \partial F^* / \partial \tau \end{Bmatrix}. \tag{6}$$

In Eq. (6), $\dot{\lambda}$ is related to the modulus of the inelastic displacement rates and $\partial F^*/\partial\sigma$ and $\partial F^*/\partial\tau$ define their directions. *F** is seen in Fig. 1, compared to *F*, and has two parts: one for compression and one for tension. For compression, only sliding is considered inelastic ($w_i = 0$). For tension, inelastic displacements will be assumed to occur in the direction of the origin of the traction space.

It can be seen that G_{IIC} does not enter explicitly in the formulation, but indirectly through friction angle ϕ (ϕ=arctan τ_{max}/σ_{max}) and β. For instance, if tan $\phi = 1$, G_{IIC} will be always greater than or equal to G_{IC}: for $\beta=1$, $G_{IIC}=G_{IC}$; for $\beta=0$, $G_{IIC}=\infty$.

2.2. The lower-bound (coupled) model

An upper-bound limit for tractions in tension can be defined combining Rankine and Guest-Tresca criteria and considering that neither σ_{max} nor τ_{max} can be exceeded by any combination of tractions. This case is depicted in Fig. 3. When material is proportionally damaged in modes I and II, cracking surface shrinks (dashed lines), until admissible area for tractions disappears. This moment corresponds to the collapse.

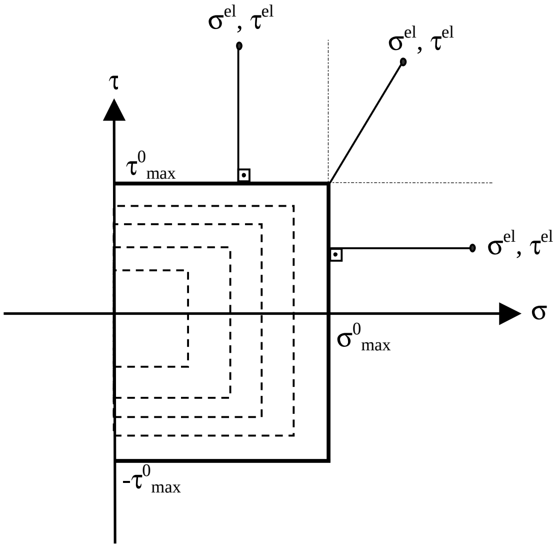

Figure 3. Upper-bound surfaces. (Vertical lines correspond to Rankine rupture surface and horizontal lines correspond to Guest-Tresca rupture surface).

The model considered here is totally uncoupled, meaning that σ_{max} is only a function of w_i (Fig. 1) and τ_{max} is only a function of v_i (the relation between τ and v used here is assumed to have the same shapes of the normal part, then, in Fig. 1, σ_{max} is replaced by τ_{max} and w_i is replaced by v_i.). An associated plasticity is used in this case, meaning that, when F>0, tractions return normally to the cracking surface. It is interesting to note that, if the return is over the Rankine part, only inelastic opening (w_i) is occurring. Near the corner, Koiter's criterion is used, meaning that elastic tractions return to the corner (see Fig. 3).

Tractions obtained in both models are rotated to global axes and spatially integrated on the cohesive surfaces. Resulting nodal forces are added to global residual forces of the finite elements. A Newton-Raphson method is used to minimize the residual forces.

3. NUMERICAL SIMULATION

The DEN plates tested by Nooru-Mohamed (1992) are used to validate the models presented in this work. The effects of mode II properties on results are also investigated. For the lower-bound model, two mode II parameters emerge, ϕ and β; for the upper-bound, ϕ is the only mode II parameter required. Plain strain conditions are assumed to prevail in both cases. The finite element used in the simulations is a constant stress triangle. Cohesive surfaces are placed between all finite elements. Tested specimen is depicted in Fig. 4(a), together with a representation of the two independent systems that apply controlled deformation (L=200 mm, a=25 mm, b=5 mm and thickness is 50 mm). In this case, tension and shear act simultaneously in order that the ratio of axial (δ) to lateral (δ_s) deformation assumes the values 1, 2 and 3. The material properties taken are the same used experimentally: E = 30000 MPa, f_{tm} = 3.76 MPa, G_{IC} = 110 N/m and poisson ratio is 0.2. The maximum coarse aggregate size is 2 mm. In the numerical model, σ^0_{max}=3.8 MPa and α=10 are used. If not mentioned otherwise, tanϕ =1.4 and β=1 are used and the softening relation by Hillerborg et al. (1976) is considered. The mesh is depicted in Fig. 4(b).

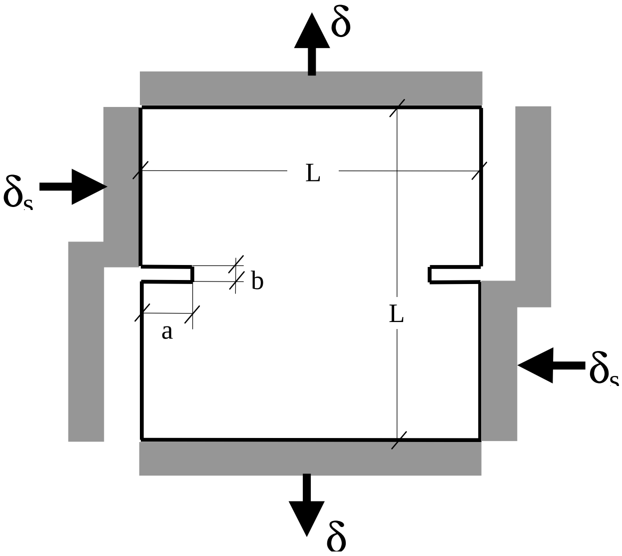

(a)

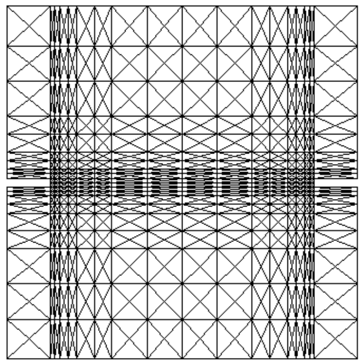

(b)

Figure 4. DEN plate (a) geometry and boundary conditions and (b) finite element mesh.

Results for the lower-bound model are initially presented. A comparison of the crack morphologies between experiments and numerical results is shown in Figs. 9(a), (b) and (c), for the ratios δ/δ_s=1, 2 and 3, respectively. Crack pattern obtained from experiments, shown at the left side in Fig. 5, indicates that the effect of shear loading on the crack propagation decreases when the ratio δ/δ_s increases from 1 to 3. In the case δ/δ_s=3, crack path is basically normal to the applied tension. Numerical results, shown at the right side in Fig. 5, present the same trend. ϕ and β parameters basically do not produce significant changes in the crack morphology. (The asymmetries observed in the solution are due to numerical rounding errors and begin when the cohesive surfaces start to collapse.)

Comparisons of the load-displacement curves with experiments also show a good agreement as indicated in Figs. 10 (only δ/δ_s=1 ratio is analyzed). Load P is calculated as the sum of the vertical reactions at the top of the plate while displacement is the axial deformation δ. It can be concluded that the larger the friction angle ϕ, the higher the peak load, but the effect becomes remarkable only for very large values of tanϕ. β has not noticeable influence in this case. The effect of the three post-peak relations described in section 3 is also illustrated in Fig. 6. The use of Hillerborg et al. (1976) softening increases peak value and gives a poorer fitting in the unloading part of the curve, when compared with the two other cases (CEB-FIP, 1993 and Xu, 1999).

Finally, the use of the upper-bound model leads to a higher values of peak loads in all three cases (δ/δ_s=1, 2 and 3). The distribution of collapsed/damaged cohesive surfaces basically does not change with the ratio δ/δ_s. Case δ/δ_s=2 and tanϕ=1.4 is illustrated in Fig. 7. The other two cases (δ/δ_s=1, 2) are not shown because they present the same morphology, indicating that the model does not capture the changes in the ratio of normal to shear loading. Values of tanϕ smaller than 1 did not improve results.

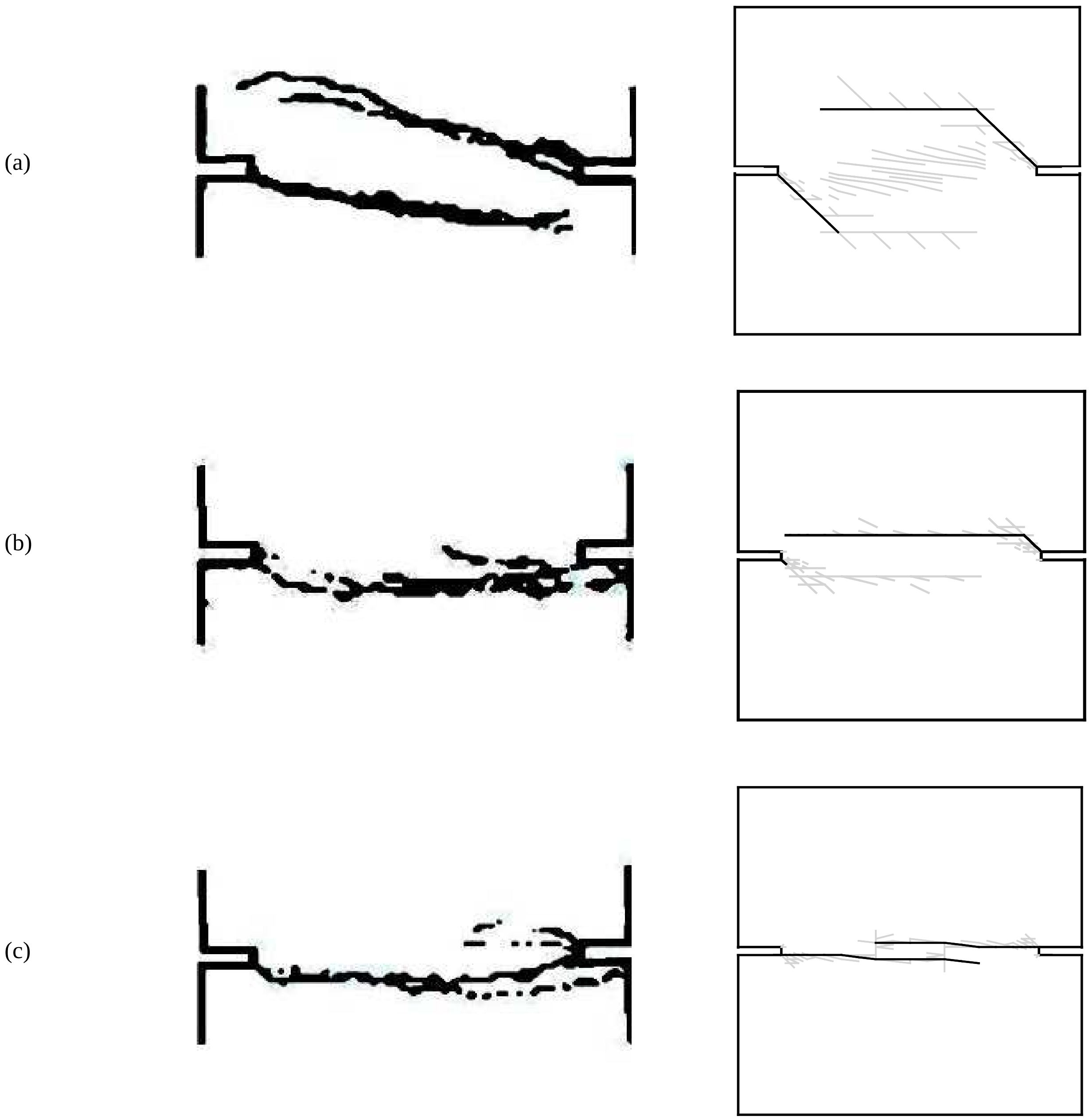

Figure 5. Crack propagation morphology. Experimental (Nooru-Mohamed, 1992) at the left side and numerical lower-bound (right side) for (a) δ/δ_s=1, (b) δ/δ_s =2 and (c) δ/δ_s =3.

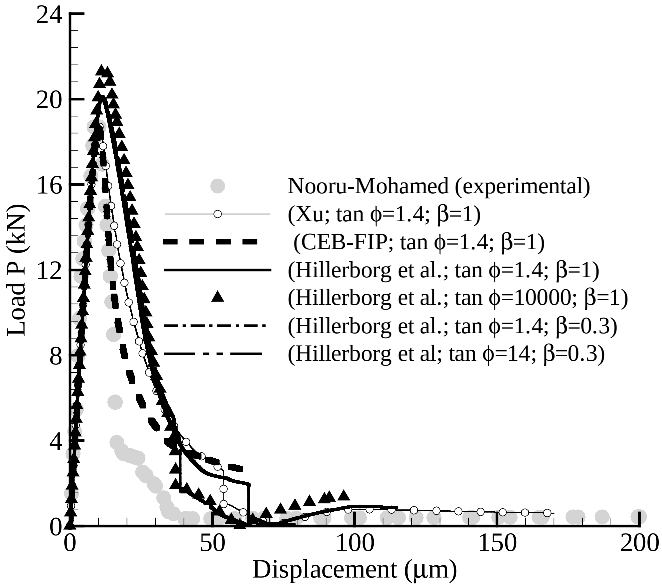

Figure 6. Load-displacement curves for the lower-bound model ($\delta/\delta_s=1$).

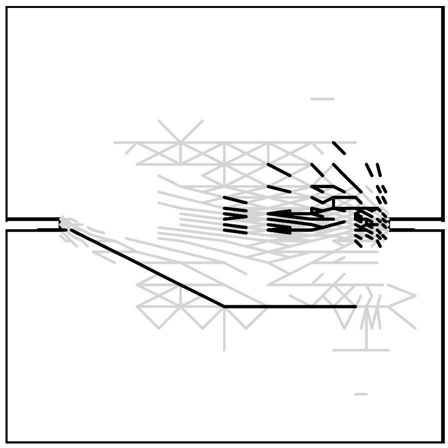

Figure 7. Crack propagation morphology for the upper-bound model (δ/δ_s=2).

4. DISCUSSION AND FINAL REMARKS

Considering the coarse meshes used in the numerical simulations presented in section 3, cohesive surfaces are not necessarily coincident with principal planes of stress. Due this fact, shear tractions are present on the cohesive zone. In this context, comparing the two models presented, only the lower-bound model was able to fit load-displacement curves and the crack pattern obtained experimentally. This occurs basically due to the way plastic correction of tractions is defined in this case: crack opening is accompanied by dissipative sliding (see Fig. 2). Dissipative sliding reduces shear tractions as expected when the crack opens. This is not the case in the upper-bound model (see Fig. 3, Rankine part). Rupture by tension, the more common situation in quasi-brittle materials, does not create any dissipative sliding. So, in this case, crack opening is accompanied by shear traction increase, which does not make sense physically.

Therefore the behavior in mixed mode fracture is linked to the return process of the elastic tractions. To verify this, the lower-bound model, with parameters tanϕ=10000 (ϕ=89.99^o) and β=0, is applied to the same example. Except for the return process, this case is almost identical to Rankine surface. However, inelastic sliding is now boosted due to assumed directions of the inelastic displacements during return (Fig. 2). This sliding reduces τ, according to Eq. (5). Contrary to Rankine with associated plasticity, results in this case present the same good fitting with experiments obtained with the lower-bound model in general.

From the discussion above, it can be implied that τ is an important variable in the numerical simulation of mixed mode fracture. Inelastic opening must be accompanied by inelastic sliding in order to reduce this traction. Clearly, the use of the associated plasticity with Rankine surface is not able to fulfill this task, because the model does not allow inelastic sliding. The attempt to constrain shear simply decreasing $\tan\phi$ for values smaller than 1 did not work out in both examples analyzed, as discussed in section 4.

It was also observed in this work that mode II parameters (ϕ, β) are almost irrelevant in the numerical results, as shown in the load-displacement curves in Figs. 7 and 10. The major effect observed was due to friction angle ϕ in the lower-bound case. It tends to increase peak load in the DEN plates case in the limit case (near 90^o) (Fig. 6). Crack pattern (Fig. 5) is also nearly independent of mode II properties. These conclusions are not new (see Gálvez et al. (2002) for instance) and can be explained by the hypothesis that, in quasi-brittle materials, collapse is in general dominated by mode I. However, the present results seem to indicate that even the shape of the cracking surface may be irrelevant and only the plastic potential used in the return process of the plastic-corrector plays a fundamental role.

5. ACKNOWLEDGEMENTS

Use of the finite element code METAFOR was possible thanks to Prof. Michel Hogge, Liège University. Author LNL thanks the Brazilian Government for support through a CAPES Fellowship and UNIOESTE for support.

6. REFERENCES

Xu, X.P. and Needleman, A., 1994, “Numerical simulations of fast crack growth in brittle solids”, J Mech Phys Solids, Vol.42, pp. 1397-1424.

Camacho, G.T. and Ortiz, M., 1996, “Computational modeling of impact damage in brittle materials”, Int J Solids Struct, Vol.33, pp. 2899-2938.

Tijssens, M.G.A., Sluys, B.L.J. and Van der Giessen, E., 2000, “Numerical simulation of quasi-brittle fracture using damaging cohesive surface”, Eur J Mech: A/Solids, Vol.19, pp. 761-779.

Basche, H.D., Rhee, I., William, K.J. and Shing, P.B, 2007, “Analysis of shear capacity of lightweight concrete beams”, Engng Fract Mech, Vol.74, pp. 179-193.

Jenq, Y. and Shah, S.P., 1988, “Mixed mode fracture of concrete”, Int J Fract, Vol.38, pp.123-142.

Bocca, P., Carpinteri, A. and Valente, S., 1990, “Size effects in the mixed mode crack propagation: softening and snap-back analysis”, Engng Fract Mech, Vol.35, pp. 159-170.

Cervenka, J. Discrete crack modeling in concrete structures, PhD Thesis, University of Colorado, 1994.

Gálvez, J.C., Cendón, D.A. and Planas, J., 2002, “Influence of shear parameters on mixed mode fracture of concrete”. Int J Fract 2002;118:163-189.

Cendón, D.A., Gálvez, J.C., Elices, M. and Planas, J., 2000, “Modeling the fracture of concrete under mixed loading”, Int J Fract, Vol.103, pp. 293-310.

Hillerborg, A., Modéer, M. and Peterson, P.E., 1976, “Analysis of crack formation and crack growth in concrete by means of fracture mechanics and finite elements”, Cement Concr Res, Vol.6, pp.773-782.

CEB-FIP, 1993, “Model Code 1990 - Bulletin d’Infornacion. Comité Euro-International du Béton”.

Xu, S., 1999, “Determination of parameters in the bilinear, Reinhardt´s non-linear and exponentially non-linear softening curves and their physical meanings”, Werkstoffe und Werkstoffprüfung im Bauwesen. Libri Bod, pp. 410-424.

Carpinteri, A., Cornetti, P., Barpi, F. and Valente, S., 2003, “Cohesive crack model description of ductile to brittle size-scale transition: dimensional analysis vs. re-normalization group theory”, Engng Fract Mech, Vol.70, pp. 1809-1839.

Bažant Z.P. and Pfeiffer P.A., 2006, “Shear fracture tests of concrete”, Mater Struct, Vol.19, pp. 111-121.

Nooru-Mohamed, M.B., 1992, “Mixed mode fracture of concrete: an experimental approach”, PhD Thesis, Delft University of Technology.

7. RESPONSIBILITY NOTICE